Canadian Science Publishing
NRC Research Press journals | Publishing Services

Canadian Geotechnical Journal
Revue canadienne de géotechnique

JOINTED PIPELINE RESPONSE TO TUNNELING INDUCED GROUND DEFORMATION

Journal:	*Canadian Geotechnical Journal*
Manuscript ID	cgj-2016-0054.R1
Manuscript Type:	Article
Date Submitted by the Author:	20-Jun-2016
Complete List of Authors:	Wham, Brad; Cornell University, Civil and Environmental Engineering Argyrou, Christina; Cornell University, Civil and Environmental Engineering O'Rourke, Thomas; Cornell University
Keyword:	pipelines, ductile iron, cast iron, tunneling ground movements, soil-pipeline interaction

JOINTED PIPELINE RESPONSE TO TUNNELING INDUCED GROUND DEFORMATION

Brad P. Wham, Christina Argyrou, Thomas D. O'Rourke

Affiliation and address:

Postdoctoral Associate, 266a Hollister Hall, Cornell University, Ithaca, NY 14853, bpw37@cornell.edu

Graduate Research Assistant, 267 Hollister Hall, Cornell University, Ithaca, NY 14853, ca353@cornell.edu

Professor, 323 Hollister Hall, Cornell University, Ithaca, NY 14853, tdo1@cornell.edu

Corresponding Author:

Brad P. Wham

266a Hollister Hall, Cornell University, Ithaca, NY 14853

Email: bpw37@cornell.edu

ABSTRACT

This paper focuses on the effect of tunneling induced ground deformation on the response of jointed cast iron and ductile iron pipelines that 1) cross the settlement profile perpendicular to the tunnel centerline, and 2) connect through 90° tees with a pipeline parallel to the tunnel centerline. The modeling involves 2D finite element analyses that account for coupled forces both parallel and perpendicular to the pipeline, and incorporates the results of large-scale laboratory tests to characterize the joints. Pipeline response is quantified with respect to joint rotation and pullout at various leakage levels as well as the allowable tensile strain. The paper describes soil displacements induced by a 6.1-m (20-ft) diameter tunnel in clay and sand. Joint rotations and maximum tensile strains for pipelines in sand exceed those in clay by up to three for the same geometric conditions. Cast iron pipelines crossing the tunnel centerline are most vulnerable to leakage from joint rotation; ductile iron pipelines have sufficient capacity against joint leakage in all cases studied. Cast iron pipelines that connect with 90° tees are highly vulnerable to leakage from pullout due to lateral soil movement. Guidance is provided for risk assessment, design, and utility operations.

Keywords: tunneling, ground movements, pipelines, cast iron, ductile iron, soil-structure interaction

Introduction

Substantial research has been performed on the characterization of ground movements caused by tunneling (Peck 1969; O'Reilly and New 1982; Mair and Taylor 1997; Marshall et al. 2012) and the influence of such movements on the response of underground pipelines (Attewell et al. 1986; Klar et al. 2005; Vorster et al. 2005; Klar et al. 2008; Wang et al. 2011). This paper expands on previous research by examining how jointed pipelines respond to tunneling induced vertical and horizontal soil movements, using the most recent research findings on the performance of ductile iron (DI) and cast iron (CI) pipelines. Ductile iron pipelines with push-on joints are widely used in current practice, whereas CI pipelines were used extensively in the past, and represent a large fraction of the current pipeline inventory of many water and some gas distribution networks.

This paper begins with an assessment of the limit states for the onset of leakage in DI and CI joints. The finite element (FE) modeling for soil/pipeline interaction is described next, with a discussion of how soil reaction normal and parallel to the longitudinal pipe axis is simulated and coupled with the rotation and pullout of the pipeline joints. Modeling of distributed vertical and horizontal soil movements caused by tunneling in clay and sand are described. The analytical results from FE soil/pipeline interaction simulations are presented and discussed for two cases involving jointed pipelines perpendicular to the tunnel centerline axis that (1) extend well beyond the width of the settlement profile and (2) connect through 90° tees with a pipeline parallel to the tunnel centerline axis. The analytical results are summarized for nominal 150-mm and 300-mm (6 and 12-in.)-diameter pipelines. Pipelines with diameters ≤ 300 mm (12 in.) comprise 99% of gas distribution pipelines in the U.S. (PHMSA 2015) and a large portion of water distribution systems. For example, approximately 90% of the water distribution system

operated by the Los Angeles Department of Water and Power involves pipe diameters ≤ 300 mm (12 in.) (Davis 2015). Recommendations are made for the identification of pipeline conditions at highest risk of leakage, modes of pipeline failure, and sensitivity of pipeline response to tunneling movements in clay and sand.

Cast Iron Pipelines

Cast iron pipelines in gas and water distribution systems were installed primarily between 1870 and 1960 (Taki and O'Rourke 1984). Pipe installed between 1870 and 1930 was manufactured predominantly by vertical pit casting to produce nominal 3.66-m (12-ft) pipe lengths; most CI pipe after 1930 was manufactured by centrifugal casting of nominal 5.50-m (18-ft) lengths.

Allowable tensile strain limits for CI pipe of 0.0005 – 0.0006 (500με – 600με) have been adopted in the Massachusetts Administrative Code, 220 CMR 113 (Massachusetts Administrative Code 2006) and waivers to 16 NYCRR, Part 255.757 (New York Administrative Code 2006) based on extensive investigations of CI pipe properties (Harris and O'Rourke 1983; Taki and O'Rourke 1984). Furthermore, numerous field tests show that a residual maximum tensile strain of 250με develops in response to pipeline installation, backfilling, and subsequent traffic loads (O'Rourke and Kumbhojkar 1984; Stewart et al. 1989). When the allowable and residual maximum strains are combined, the resulting strain is less than one-fourth the average failure strain that was measured in pit cast iron tensile test specimens taken from pipelines after 50 to 80 years in the field (Taki and O'Rourke 1984). A lower limit of 500 με is appropriate for centrifugal CI pipe, which in some instances may be vulnerable to stress crack corrosion (Taki

and O'Rourke 1984). The upper limit of 600με used in this work is applicable for pit cast iron pipe, which is representative of the majority of CI pipelines in current service.

Tensile test data for CI pipe from Johnson (1890), Schlick and Moore (1936), and Taki and O'Rourke (1984) show a range of CI modulus from 75.8 to 128 GPa (11,000 to 18,500 ksi). A secant modulus, E, of 75.8 GPa (11,000 ksi), which is strain compatible with both the allowable and the combined allowable and residual maximum tensile strain, is used in this study (Wham 2016).

Axial Force vs. Displacement of CI Joints

Figure 1 shows a profile view of a typical CI joint, which connects the spigot and bell ends of adjoining pipes. The annular space between the spigot and bell is packed with hemp or jute yarn and predominantly lead or cement caulking. Prior (1935) indicates that the lead caulking depth is typically 57 mm (2.25 in.), while Attewell et al. (1986) report depths of 44 to 57 mm (1.75 to 2.5 in.), depending on diameter. This work focuses on CI joints with lead caulking and soft hemp or jute, typical of most water and some gas distribution pipelines. Such joints are less resistant to pullout and more flexible in rotation than cement-caulked joints and joints in gas mains where the yarn is often impregnated with hardened hydrocarbons (Harris and O'Rourke 1983).

The relationship between joint pullout force at first slip, $F_{j,slip}$; CI-lead adhesion, C_A; and joint geometry is

$$F_{J,slip} = \pi D_{os} d_L C_A \qquad (1)$$

where D_{os} is the outer spigot diameter and d_L is the lead caulking depth as illustrated in Fig. 1.

Through Eqn. 1 the C_A corresponding to first leakage was calculated from the results of 15 pullout tests under internal water pressure ranging from 140 to 2500 kPa (20 to 360 psi) on specimens of lead caulked CI joints ranging from 150 to 1500 mm (6 to 60 in.) in nominal diameter (Prior 1935), as well as two similar specimens of nominal 300-mm (12-in.)-diameter CI joints tested under nitrogen pressure of 2.0 kPa (0.29 psi) (O'Rourke et al. 1996). All tests were conducted for a lead caulking depth of approximately 57 mm (2.25 in.). Detailed information about the joint pullout tests and tabulation of experimental data is provided by Wham (2016).

Figure 2 shows a cumulative frequency plot of the C_A data and a cumulative probability curve, developed from the mean and standard deviation of the data. The Lilliefors (1967) goodness of fit test shows that a normal distribution is verified at the 5% significance level, and thus is a suitable fit of the data.

Figure 3 shows the normalized force vs. displacement plots for five typical pullout tests, including two with internal gas pressure and three with internal water pressure. The measured axial force is normalized with respect to the pullout force at first leakage. Due to limitations of measuring methods used by Prior (1935), initial joint stiffness data at displacements less than 0.79 mm (0.031 in.) are not reliable. The O'Rourke et al. (1996) pull-out tests offer the most detailed data available for assessing initial joint stiffness and provide the basis for the idealized axial pullout curve shown as a dashed line in the figure. A well-defined break in the slope of these curves occurs at 0.51 mm (0.02 in.), after which there is variation in the normalized force vs. displacement relationships.

The inset diagram in the figure shows an expanded view of the normalized force vs. axial displacement plots at low levels of movement. There is a clear transition to a flatter slope at

about 0.50 mm (0.02 in.). This displacement occurs at the onset of leakage and corresponds to a notable change in the rate at which resistance is mobilized against pullout. This slip between the lead and CI surface generates leakage paths. As discussed by O'Rourke et al. (1996), continued deformation of lead caulking can actually close off leakage paths after initial leakage. Thus, slip at the onset of leakage can be identified at 0.50 mm, but a clear and consistent trend in leakage with additional pullout cannot be quantified with the current experimental evidence.

Moment vs. Rotation of CI Joints

Harris and O'Rourke (1983) explored the relationship among moment, rotation, and leakage with four point load tests of CI joints with nominal diameters of 100, 150, and 200 mm (6, 4, and 8 in.) under nitrogen pressures of 3.0 kPa (0.43 psi) consistent with the operation of low pressure gas mains. These joints were sampled from the field after 50-80 years of operation. Figure 4 presents the data from 19 tests on lead-caulked pit CI joints expressed as leakage vs. joint rotation for 10% through 90% exceedance limits. Each plot represents the leakage at which a particular percentage of the test specimens exceeds the leakage rate shown. The total number of specimens at each stage of testing is plotted with respect to rotation. As the rotation increased, some tests were discontinued because pipes fractured or loads exceeded safety limits adopted for the tests, thereby reducing the number of specimens.

The onset of leakage occurs at approximately 0.2°, with maximum leakage at approximately 0.5°. There was actually a decline in leakage at all exceedance levels after 0.5°. Leakage eventually increased at large rotations exceeding 3-4° (not shown in the figure) in those joints that did not fail. No pipe failures were observed until about 0.5°, after which there was an increase in the number of failures as rotation increased.

O'Rourke and Trautmann (1980) proposed an equation for the moment at first slip between the lead and CI surface, $M_{J,slip}$, in which C_A, d_L, and D_{os} are as defined for Eqn. 1, as follows

$$M_{J,slip} = \frac{3}{8} \pi D_{os}^2 C_A d_L \qquad (2)$$

Using Eqn. 2 with the mean C_A from Fig. 2 and d_L = 57 mm (2.25 in.), normalized moment vs. rotation plots were developed from four bending tests on nominal 500-mm (20-in.)-diameter CI joints with no internal pressure (Prior 1935) and nominal 150-mm (6-in.)-diameter CI joints under 3 kPa (0.43 psi) gas pressure (Harris and O'Rourke 1983). The plots are shown in Fig. 5 in which the measured bending moment is normalized with respect to the moment at first leakage, calculated with Eqn. 2. In Fig. 5(a) a change in the normalized moment vs. rotation plots can be identified at about 0.2°. Both O'Rourke and Trautmann (1980) and Rajani and Abdel-Akher (2013) attribute this change in slope to deformation of the lead caulking, related to first slip between the lead and CI surface, that generates leakage.

Figure 5(b) is an expanded view of the normalized moment vs. rotation plots to 0.6° rotation. The rotation, corresponding to a prominent slope reduction in the plots, varies between 0.1 and 0.4°. Initial joint stiffness for the generalized curves is given by $k_1 = M_{j,slip}/\theta_1$ where $M_{j,slip}$ is calculated from Eqn. 2 assuming a mean C_A and d_L = 57 mm (2.25 in.), and θ_1 = 0.2° where θ_1 is the rotation at first slip. As recommended by Rajani and Abdel-Akher (2013), beyond 0.2° of rotation the initial joint stiffness is reduced by 75% for diameters less than 400 mm (16 in.), and 65% for larger diameters. Based on the available test data, a third change at 1.0° was adopted to reduce the slope of the curve to 12% and 20% of the initial stiffness for 150 and 500-mm (6 and 20-in.)-diameter joints, respectively.

Ductile Iron Pipelines

Ductile iron pipe in U.S. practice conforms to the ANSI/AWWA C151/A21.51 standard (AWWA 2009). Typical stress vs. strain data from direct tension tests on pipe specimens of commercial grade DI are reported by Wham and O'Rourke (2015) and used in this work. The average ultimate strength of 460 MPa (66.7 ksi), yield strength of 311 MPa (45.1 ksi), strain at failure of 10.4%, and average elastic modulus of 186,000 MPa (27,000 ksi) obtained from those tests exceed minimum standard requirements.

The DI pipelines most frequently used in water distribution systems are equipped with push-on joints for ease of installation. A typical 150-mm (6-in.) DI joint, which connects the spigot and bell ends of adjoining pipes, is shown in Fig. 6. An elastomeric gasket provides a watertight seal. As illustrated in the figure, the maximum joint rotation before metal to metal contact, or metal binding, is nominally 5° when the spigot is inserted into the full depth of the bell.

Wham and O'Rourke (2015) developed a relationship among leakage, rotation, and moment at various levels of axial displacement from the results of 22 tests on DI joints with a nominal diameter of 150 mm (6 in.) under 380 kPa (55 psi) of internal water pressure. The relationship at first leakage is shown in Fig. 7 as normalized joint rotation (rotation divided by rotation at metal binding, 5°) vs. normalized pullout (axial displacement from the position of a fully inserted spigot divided by the maximum pullout, 51 mm (2 in.)). The experimental results are plotted for two combinations of normalized rotation and pullout at which there is metal binding and first leakage. Simplified, approximate limit states for metal binding and leakage are shown by the continuous and dashed lines, respectively.

The dashed line represents the pressure boundary for DI joints included in this study. Any combination of normalized rotation and pullout on and above this line coincides with joint

leakage. Wham and O'Rourke (2015) show that the pressure boundary is independent of load path and can be used for many different conditions of evolving rotation and pullout associated with complex ground deformation patterns.

Although Fig. 7 is presented in terms of normalizing parameters, it is not intended for the 150 mm (6 in.) joint pressure boundary to be used for all DI pipe diameters and commercially available configurations. Additional experimental testing or 3D FE analysis, as outlined by Wham and O'Rourke (2015), is needed to establish larger diameter joint response to combinations of joint pullout and rotation.

Soil Pipeline Interaction Model

Analytical models for underground pipeline response to tunneling induced ground movements have been developed and calibrated by centrifuge tests for continuous and jointed pipelines, applying linear equivalent and elastoplastic formulations for soil-pipe interaction (Klar et al. 2005; Vorster et al. 2005; Klar et al. 2007; Klar et al. 2008; Klar and Marshall 2015). Models developed by Marshall et al. (2010) account for changes in soil stiffness arising from out-of-plane shear strains in combination with those at the pipe level, and provide the best predictions of pipe bending moment compared to centrifuge test results.

An alternative approach was adopted in this work following the procedures recommended for analyzing pipeline response to earthquake induced ground deformation (ASCE 1984; Honegger and Nyman 2004; O'Rourke et al. 2008). A detailed description of this methodology for characterizing soil-pipe force vs. displacement relationships in sand is provided in this special issue by Jung et al. (2016).

Figure 8 illustrates the basic concept of the modeling process for a continuous pipeline in which the pipe is modeled as a beam, often with both nonlinear material and geometric properties. Although only bi-linear relationships are presented in the figure, soil-pipe interactions orthogonal and parallel to the pipeline longitudinal axis can be modeled by linear, multi-linear, or nonlinear relationships derived from full-scale laboratory tests of soil-pipe interaction (O'Rourke 2010; Jung et al. 2013a and b). For example, Jung, et al. (2016) explain how soil-pipe force vs displacement in sand can be modeled as bilinear and nonlinear relationships, using a rectangular hyperbola to represent nonlinear conditions. The primary advantage of this approach is that the characterization of nonlinear soil-pipe interaction is based on the measured performance of real pipe under burial conditions that replicate those in the field. Moreover, the method is expanded in this work to account for the fully coupled interaction between soil forces normal and parallel to the longitudinal axis of the pipeline as well as the axial force vs. displacement and moment vs. rotation relationships of CI and DI joints previously discussed. Thus, the methodology is comprehensive and, although it does not account for soil continuity that is captured by other well-known approaches (Klar et al. 2005; Vorster et al. 2005), its versatility and fidelity to real soil-pipe interaction and pipe joint behavior in the field have substantial merit.

Figure 9 presents a schematic of the enhanced soil-pipeline interaction model with pipe elements, joints, and connection to a 90° pipeline tee. The tee is simulated by a single node with known boundary conditions. Displacements representing vertical and lateral soil movements caused by tunneling are conveyed to the nodes at the far sides of the soil spring elements, thus simulating soil interaction with the pipe. Pipeline joints are modeled by rotational and axial relationships developed from large-scale laboratory tests. The transverse spring stiffness is set to

a very high value, which simulates contact and transfer of shear force between the spigot and bell.

The modeling approach is readily implemented in commercially available FE software. In this work the general purpose FE software ABAQUS (2014) was used for 2D FE modeling in which the pipeline is represented by beam elements (type b33) and the soil resistance normal to the pipeline axis by nonlinear springs (type spring2). The springs are connected to the pipeline with uniaxial gap elements (type gapuni) that transfer forces parallel and perpendicular to their axes only when the corresponding normal springs carry compressive forces. This is achieved by allowing separation of the gap elements when tensile normal forces are activated in response to load relaxation and separation between soil and pipe.

The force per unit distance transferred through the gap element parallel to the pipeline longitudinal axis is controlled by the Coulomb friction law so it is proportional to the normal force acting on the pipeline at each level of deformation. As an initial step, the displacements required to activate the normal forces for at-rest conditions are imposed on the transverse springs. With this adjustment, longitudinal frictional forces are activated to reflect at-rest conditions in the absence of normal forces triggered by relative soil displacement normal to the pipeline longitudinal axis. During simulation, incremental parallel and normal soil movements are applied simultaneously at the longitudinal and transverse spring nodes on each side of the pipeline elements.

Ground Movement Characterization

The settlement profile caused by tunneling under greenfield conditions in undrained clay, where the soil exhibits constant volume deformation, has been shown by numerous investigators (Peck 1969; O'Reilly and New 1982; Mair and Taylor 1997) to match a Gaussian curve of the form

$$S_v(y) = S_{v,\max} \exp\left[\frac{-y^2}{2i_z^2}\right] \qquad (3)$$

for which $S_v(y)$ is settlement at distance y from the centerline, $S_{v,max}$ is maximum centerline settlement, and i_z is horizontal distance from the tunnel centerline to the inflection point of the Gaussian curve at a depth z_o above the tunnel centerline, as illustrated in Fig. 10. The value of $i = Kz_o$, where K is an empirical constant related to ground conditions.

To account for decreasing i with depth, Mair et al. (1993) proposed an equation that was expressed by Marshall et al. (2012) as

$$K = \frac{K_s + (\partial i / \partial z)(z_p / z_t)}{1 - z_p / z_t} \qquad (4)$$

where the trough width parameter is defined relative to K at the surface, K_s; the slope of i in relation to depth, $\partial i/\partial z$; distance from the ground surface to depth of interest, z_p; and distance from the ground surface to the depth of the tunnel axis, z_t. Mair et al. (1993) recommended $K_s = 0.5$ and $\partial i/\partial z = -0.325$ for clays, while Mair and Taylor (1997) show that K_s ranges typically from 0.25 to 0.45 for sands and gravels based on field measurements.

To conform to constant volume deformation, the magnitude of horizontal ground movement, S_h, is commonly expressed by the following relationship

$$S_h = \frac{y}{z_R} S_v \qquad (5)$$

where y is the horizontal distance from tunnel centerline and z_R is the distance from the depth of interest to the radial focal point of ground movement vectors. The maximum horizontal displacement, $S_{h,max}$, occurs at the settlement trough inflection point, i_z, as illustrated in Figure 10.

To characterize ground movement in undrained clay, O'Reilly and New (1982) set $z_R = z_o$, which implies that vectors of ground movement are directed toward the tunnel axis. The few available case studies that provide reliable measurements of S_h indicate that the focal point of the ground vectors varies, and for constant volume conditions, may be below the tunnel axis (Cording, 1991; Hong and Bae 1995).

O'Reilly and New (1982) show by integration of Eqn. 3 that $S_{v,max}=V_{ls}/(i_z\sqrt{2\pi})$ where V_{ls} is the volume of the settlement profile per unit advance. Combining this relationship with Eqns. 3 and 5 provides expressions representing the vertical, $S_v(y,z)$, and horizontal, $S_h(y,z)$, components of ground displacement across the transverse cross-section of the tunnel, as follows

$$S_v(y,z) = \frac{V_{ls}}{i_z\sqrt{2\pi}} \exp\left[\frac{-y^2}{2i_z^2}\right] \qquad (6)$$

$$S_h(y,z) = \frac{y}{z_R}\frac{V_{ls}}{i_z\sqrt{2\pi}} \exp\left[\frac{-y^2}{2i_z^2}\right] \qquad (7)$$

Field measurements and centrifuge test results (Lake et al. 1996; Mair and Taylor 1997; Osman et al. 2006) confirm that the Gaussian settlement profile is well represented for tunneling in clays. Because of constant volume deformation in clay, the short-term settlement profile volume, V_{ls}, remains equal to volume loss at the tunnel. A notable exception pertains to

consolidation-induced volume loss caused by increased effective stresses resulting from long-term drainage into the tunnel (Lake et al. 1996; Mair and Taylor 1997).

Tunneling induced volume losses in sand are considerably more complex than those in clay. Field measurements (Cording and Hansmire 1975; Cording 1991) and centrifuge test results (Marshall 2009; Marshall et al. 2012, and Zhou 2014) show that volume changes in sand are influenced by depth, tunnel depth relative to diameter, volume loss at the tunnel, and soil density. In contrast to clay, the assumption of constant volume loss in sands will underestimate volume loss near the ground surface when loss in the tunnel is less than 1% and overestimate when tunnel volume loss exceeds 2-3% (Marshall et al. 2012; Zhou 2014).

Selection of Vertical and Lateral Displacement Profiles

This paper concentrates on pipeline response to tunneling induced settlement and lateral displacement transverse to the tunnel centerline. Mair and Taylor (1997) note that the longitudinal settlement trough along a tunnel centerline in clay can be estimated with a cumulative probability curve where the maximum settlement is the same as that in the transverse settlement trough. Cording (1991) reports that the average slopes of both the longitudinal and transverse settlement troughs were approximately equal for tunnels driven in the sand and gravel terrace deposits of Washington, DC. Lake et al. (1992) report that the maximum slope, curvatures, and horizontal strains for the longitudinal settlement profiles are significantly less than those values for the transverse settlement trough as calculated for tunnels in many different soil conditions.

On the basis of these observations, the most severe conditions of soil-pipeline interaction are likely to be along the transverse settlement profile, with ground movement effects equal to or less than those in the transverse section for all other pipeline orientations with respect to the tunnel centerline. This generalization is corroborated by Lake et al. (1992), who note that the transverse trough will usually represent the highest risk of damage to a structure.

In this work transverse settlement and lateral displacement profiles were selected to represent relatively high levels of ground deformation for tunnels with a low soil cover to tunnel diameter ratio, C/D, which is defined as the distance from ground surface to tunnel crown divided by the excavated tunnel diameter. Soil movement profiles were chosen for C/D = 1.15 and a 6.1 m (20 ft) tunnel diameter in clay and sand, consistent in size to a rapid transit tunnel. A pipeline depth, z_p, of 0.9 m (36 in.) was chosen to represent typical burial conditions for pressurized pipelines with $D_p \leq 300$ mm (12 in.). The intention is to subject CI and DI pipelines to relatively high levels of deformation to guide design and risk assessment and help identify potential difficulties.

Settlement and horizontal displacement profiles consistent with Eqns. 6 and 7 were used along the pipeline, where $i = Kz_o$ and K = 0.5 in clay, and K = 0.28 in sand (Mair et al. 1993; Marshall 2012). Tunnel volume loss in clay was limited to 5% of the tunnel cross-section as a practical upper bound. Tunnel volume loss in sand was limited to 3% to avoid conditions that promote concentrated settlement near the centerline and deviation from a Gaussian settlement distribution (Cording 1991; Marshall et al. 2012). Centrifuge test results for medium to dense sand (Marshall et al. 2012; Zhou 2014) show that surface and tunnel level volume losses are relatively close when tunnel losses are less than 3%.

The focus of this work is on detailed modeling of pipeline and soil-pipeline interaction with estimates of vertical and horizontal movement suitable for practical use. Alternative mathematical formulations have been proposed for modeling the distribution of tunneling induced settlement (Vorster et al. 2005; Marshall et al. 2012), but an evaluation of these expressions is beyond current scope.

Pipeline Crossing the Width of the Settlement Profile

Analytical results are presented for a CI pipeline with 3.6-m (12-ft)-long segments for both joint centered (JC) and pipe centered (PC) locations relative to the tunnel centerline, as illustrated in Fig. 11. The maximum joint rotations occur at the tunnel centerline for the JC configuration, and the maximum pipe bending occurs at the tunnel centerline for the PC configuration. These configurations set bounding conditions on the most severe joint rotations and bending strains.

In all cases, it was assumed that the pipelines are buried in granular backfill of limited depth ($\leq$ 2 m) with elasto-plastic force vs. displacement characteristics typical of dense sand (Jung et al. 2013a and b; O'Rourke et al. 2015). The analytical results converged for element lengths $\leq$ 75 mm (3 in.) and total number of 3.7-m (12-ft) CI or 5.5-m (18-ft) DI pipe lengths between 10 and 14, depending on the pipeline configuration. The total number of beam, spring, and gap elements varied from 4,815 to 7,167 depending on pipeline composition and configuration.

Cast Iron Pipelines in Clay

In Figs. 12(a), (c), and (d) and Fig. 12(b) the maximum joint rotation and tensile strain, respectively, are plotted relative to the centerline settlement, $S_{v,max}$, in clay. The maximum tensile strain was determined from the addition of the axial and bending strains at all locations along the pipeline.

Figure 12(a) shows maximum joint rotation vs. centerline settlement for 150-mm (6-in) and 300-mm (12-in.)-diameter pipelines with JC and PC configurations. For a given settlement and pipe diameter, the maximum joint rotation for a JC configuration always exceeds that for a PC configuration. For the same settlement, the rotations of the 300-mm-diamter pipelines more than double those of the 150-mm-diameter pipelines. The initiation of joint leakage at 0.2° rotation in 150-mm-diamter pipelines occurs between 100 and 125 mm (4 and 5 in.) of centerline settlement. Joint leakage initiation in 300-mm-diameter pipelines occurs between 50 and 75 mm (2 and 3 in.) of centerline settlement. Only the 300-mm-diameter JC pipeline exceeds the 0.5° maximum leakage threshold.

Figure 12(b) shows the maximum tensile strain vs. centerline settlement. In all cases the tensile strains are below the allowable limit. Similarly, the pullout displacement in all cases is below the axial movement associated with initial joint leakage. Typical pullout displacements are shown for CI pipelines in sand under the next heading.

Figure 12(c) demonstrates the sensitivity of joint rotation to the modulus of the CI pipe. As the modulus increases from 76 to 128 GPa (11,000 to 18,500 ksi), the maximum joint rotation increases for the same $S_{v,max}$. Figure 12(b) shows little change in tensile strain in the 150-mm-diameter pipeline for a given settlement, reflecting nearly constant bending moment for the range

of E pertaining to pit and centrifugally cast iron. For small strains, the pipe curvature $\kappa = M/EI$ where M, E, and I are the moment, modulus, and moment of inertia of the pipe. Since M does not change with E, the curvature, κ, decreases as E increases. Less pipe curvature results in increased joint rotation, as illustrated in the figure.

Figure 12(d) shows maximum joint rotation vs. centerline settlement for a 150-mm-diameter pipeline with a JC configuration. The different plots correspond to the mean as well as the 10%, and 90% exceedance levels, associated with the normal cumulative distribution of CI-lead adhesion, C_A, plotted in Fig. 2. For a given level of settlement, the strongest and stiffest joints with 90% exceedance levels for C_A reduce rotation by about one third relative to the weakest joints with 10% exceedance levels. The figure also shows the rotations for joints with no rotational stiffness, thus setting an upper bound for rotation. The moment mobilized in CI joints reduces rotation to about half the value associated with zero-moment, or pinned, connections.

Cast Iron Pipelines in Sand

Figure 13 shows plots similar to those in Fig. 12 for CI pipelines in sand. Tunneling in sand results in a narrower settlement profile with i = 2.6 m (8.5 ft), nearly one-half i = 4.73 m (15.5 ft) for clay. As expected for a narrower settlement profile, CI joint rotations are larger than those for the same centerline settlement in clay for similar size pipe and joint configuration (i.e., JC and PC conditions). Figure 13(a) shows that, for a given settlement and pipe diameter, the maximum joint rotation for a JC configuration always exceeds that for a PC configuration. The same trend is shown in Fig. 12. Of particular note, the centerline settlements decrease for limit state rotations of 0.2° and 0.5°. The centerline settlements, which trigger maximum leakage at 0.5°,

are as low as 30 and 60 mm (1.2 and 2.4 in.) for 300-mm and 150-mm-diameter pipelines, respectively.

Figure 13(b) shows the maximum tensile strains vs. centerline settlement. Consistent with the trends in Fig. 12, maximum tensile strains are larger than those for the same centerline settlements in clay for similar size pipe and joint configurations. The allowable tensile strain of 600με is exceeded for PC configurations at approximately 55 and 60 mm (2.2 and 2.5 in.) centerline settlement for 150-mm and 300-mm-diameter pipelines, respectively. Similar to the results for clay, the pullout displacements in all cases are below the axial movement associated with initial joint leakage, and are not plotted in the figure.

Of particular interest is the PC case for the 300-mm-diameter pipe, where the trend in centerline settlement vs. maximum tensile strain changes abruptly at about 50 mm of settlement with a marked reduction in the rate of increase in the strain vs. settlement. To understand this response, Fig. 14(a) shows the greenfield and pipeline settlement profiles for maximum centerline settlements of 25 mm and 125 mm. The deformed shape of the pipeline conforms to the settlement profile for low values of settlement, but transitions starting at 35 mm to the response depicted for 125 mm maximum settlement, where settlement of the central pipe section lags behind that of the ground.

The soil reaction forces per meter along the pipeline are plotted in Fig. 14(b). The reaction forces attain their maximum uplift capacity in the central pipe section. The maximum pipe flexure and bending moment do not increase in the central pipe section, and thus the maximum pipe tensile strain shows little increase after 35 mm centerline settlement. At 125 mm maximum

settlement, the uplift reaction attains its maximum value at the second pipeline joint from the centerline, where upward deformation and joint rotation occur.

As shown in Fig. 14(c), the maximum tensile strain in the central pipe section increases from a maximum settlement of 25 mm to 125mm, but the rate of increase is reduced after 35 mm centerline settlement due to the relatively constant soil reaction force/m on the central pipe section. The tensile strains increase outside the inflection point of the settlement profile, where concave curvatures of the pipeline and settlement profile are increasing. At 125 mm of centerline settlement the tensile strains inside and outside the inflection point are nearly equal. At larger centerline settlement the maximum tensile strain occurs outside the inflection point.

Ductile Iron Pipeline in Sand

Figure 15 presents the maximum joint rotations and tensile strains for 150-mm-diameter DI pipelines in sand vs. centerline settlements. Given the high capacity for rotation, high yield strength, and ductility of DI pipelines, the more severe ground deformation associated with sand was selected for analysis. Three joint configurations were evaluated, including JC, PC, and an intermediate case where the DI joint is offset one quarter of the 5.5-m (18-ft) pipe length from the tunnel centerline.

In all cases, joint rotations are well under the limits for metal binding and far less than the rotational capacity at first leakage. The maximum joint pullout (not shown) was less than 5 mm (0.2 in.), well below the 50 mm (2 in.) allowable pullout for joint leakage. Likewise, the tensile strains are well below the 3500με associated with the yield stress of DI pipe (ASTM 2015). For

the 125-mm maximum settlement, the maximum bending strain is less than the 1500με proportional limit of DI (maximum strain for constant E).

Pipelines with Tees

Figure 16 shows a transverse cross-section of a tunnel and settlement profile affecting a branch pipeline connected through a 90° tee to another pipeline parallel to the longitudinal axis of the tunnel. A plan view of the tee and interconnecting parallel and branch pipelines is also shown.

Figure 17 presents a simplified 3D view of the tee. A concrete thrust clock is often placed adjacent to the tee to resist unbalanced force from internal water pressure. For CI pipelines and tees the thrust block resistance and torque combined from the two joints connecting with the parallel pipeline will resist the overturning moment at the joint induced by differential settlement of the branch pipeline. As discussed by Wham (2016) the tee tends to settle without rotation for both CI and DI pipelines and tees. Thus, no rotation of the tee was assumed in the FE simulations.

Cast Iron Tees

By extracting the maximum pullouts, rotations, and tensile strains from multiple simulations of tunneling movement effects on tees at different distances with respect to the tunnel centerline, the centerline settlements associated with joint pullout and rotational limits were identified and plotted with respect to tee location from the centerline in Figs. 18(a) and (b) for tunneling in clay and sand, respectively. Following a similar approach, the centerline settlements required to develop the allowable CI tensile strain are plotted in Fig. 19.

In Figs. 18(a) and (b) a range of 0.5 to 1.0 mm (0.02 to 0.04 in.) is used to bracket the axial slip at first leakage. For both clay and sand, the CI tees are susceptible to pullout-related leakage at low centerline settlements of approximately 10-15 mm (0.4-0.6 in.) when the tee is located between horizontal distances of 0.5i to 2i from the tunnel centerline. Low settlements of about 15 mm (0.6 in.) are associated with rotation at first leakage in sand when the tee is located a horizontal distance i from the tunnel centerline. For all cases in Figure 19 the centerline settlements required to exceed the allowable CI tensile strain are well above those that exceed the pullout and rotational limit states.

Figure 18 shows high susceptibility to leakage from pullout when CI tees are located between 0.5i and 2i from the tunnel centerline. The maximum tunnel settlements associated with the initiation of leakage are sufficiently low that tee locations anywhere within the settlement trough (≅ 2.5i) should be regarded as highly vulnerable to tunneling induced movement.

Ductile Iron Tees

To explore the susceptibility of DI tees to pullout, the analytical results for maximum pullout at 120-mm (4.8-in.) of centerline settlement is plotted with respect to tee location in Fig. 20. The tee location is expressed in terms of horizontal distance from the tunnel centerline normalized by i for clay and sand. Both an unrestrained tee and a tee restrained from pullout at its connection with a 150-mm-diameter branch pipeline were modeled.

Figure 20 shows that maximum pullout occurs when the tee is at or near the inflection point, i, in all cases simulated. At all tee locations the maximum pullout is slightly higher in sand than clay. The largest pullouts occur for restrained tees at the next joint of the branch pipeline.

Restraining the tee from pullout actually reduces the degrees of freedom available in the branch pipeline to accommodate lateral ground movement. Thus, more separation is induced in the branch pipeline joints for a restrained vs. an unrestrained tee.

All analytical results for DI tees were examined for combined joint pullout and rotation and compared with the metal binding and pressure boundaries presented in Fig. 7. Although some limited cases show pullout on the order of 70 to 80% of push-on joint pullout capacity, all combinations of pullout and rotation were below both the metal binding and pressure boundaries in Fig. 7.

Conclusions

The response of jointed CI and DI pipelines to tunneling induced ground deformation is evaluated for pipelines that 1) cross the width of settlement profile perpendicular to the tunnel centerline, and 2) connect through 90° tees with a pipeline parallel to the tunnel centerline. The modeling involves 2D finite element analyses that account rigorously for coupled forces both parallel and perpendicular to the pipeline, and incorporates the results of large-scale laboratory tests to characterize the axial force vs. displacement and moment vs. rotation relationships of DI and CI joints commonly encountered in practice. Tunneling induced soil displacement profiles were modeled for a 6.1-m (20-ft)-diameter tunnel in clay and another in sand with a cover to depth ratio, C/D, of 1.15 affecting 150-mm and 300-mm (6 and 12-in.)-diameter CI and DI pipelines.

The research findings reported herein are directly applicable to CI and DI pipelines with nominal diameters less than or equal to 300 mm (12 in.), which covers over 90% of water distribution and 99% of gas distribution pipelines in the U.S. General results from the research

can be used to guide risk assessment, design, and utility operations for pipelines as large as 600 mm (24 in.) in nominal diameter.

With respect to jointed CI and DI pipeline performance, the principal observations and conclusions are

- The limit states for first leakage in lead-caulked CI joints are related to measured deformation, or slip, between the lead and CI surfaces within the joints at 0.5 mm (0.02 in.) of axial pullout and approximately 0.2° of joint rotation. Moment vs. rotation test results for 100-mm, 150-mm, and 200-mm (4-in., 6-in. and 8-in,)-diameter lead-caulked CI joints taken from the field after 50 to 80 years of operation show that leakage under typical operating pressure peaks initially at about 0.5° rotation and declines thereafter until leakage again increases at rotations in the range of 3 to 4°.
- Equations for evaluating the CI pullout force and moment at first leakage are provided, which are related to the CI-lead adhesion, C_A. Data for C_A from large-scale pullout tests are shown to follow a normal distribution, thus allowing for the quantification of uncertainty in pullout force and moment to initiate leakage.
- The CI joints display complex behavior in which additional slip and creep of the lead can close off leakage paths that are reopened with further increase in deformation. Thus, the slip and rotation at incipient leakage can be identified, but a clear and consistent trend in leakage after its initiation cannot be quantified with the available experimental evidence.

For jointed CI and DI pipelines that extend beyond the width of the settlement profile, the principal observations and conclusions drawn from the analytical results are:

- Pipeline response evaluated in this work corroborates the findings of many other investigators (Attewell et al. 1986; Klar et al. 2005; Wang et al. 2011) that both joint rotations and pipe strains are sensitive to i, the horizontal distance from the tunnel centerline to the inflection point of the settlement trough. Moreover, since i tends to be smaller in sands relative to clays for the same tunnel diameter and depth, pipelines will be more vulnerable in sands for the same centerline settlement, tunnel diameter, and depth conditions. This work, although focused on limited tunnel size and depth considerations, helps to quantify pipeline and tee response to i by using detailed full-scale test data and modeling of CI and DI limit states. Additional investigation of pipeline response to variations in i and other ground movement parameters, using the pipeline limit states in this work, is recommended.
- The response to tunneling in sand is accompanied by joint rotations and maximum tensile strains that exceed those in clay by a factor as high as two to three for the same centerline settlement and pipe diameter. This difference is related to the narrower settlement profile and smaller i in sand that generate larger differential settlements and curvatures.
- For the tunneling conditions examined in this work, CI joint rotation at first leakage in clay occurs between 50 and 120 mm (2.0 and 4.8 in.) of centerline settlement, and depends on both the pipe diameter and location of the joints with respect to tunnel centerline. For sand the threshold of incipient leakage is exceeded at centerline settlements on the order of 25 mm (1 in.).

- Allowable tensile strain levels for pit cast iron pipe were not exceeded for centerline settlements in clay as high as 120 mm (4.8 in.), but were exceeded at centerline settlements in sand of approximately 50-100 mm (2-4 in.).
- For DI pipelines joint rotations were well under the limits for metal binding and far less than the rotational capacity at first leakage. Joint pullout was minimal, and maximum tensile strains were below yield conditions.

For jointed pipelines, which connect through 90° tees with a pipeline parallel to the tunnel, the principal observations and conclusions are:

- The susceptibility to leakage from pullout when CI tees are located between 0.5i and 2i from the tunnel centerline (where i is the location of the settlement profile inflection point) is sufficiently low that tee locations within the settlement trough (≅ 2.5i) should be regarded as highly vulnerable to the effects of tunneling.
- The largest pullouts for DI pipelines with unrestrained and restrained tees occur at a distance close to the inflection point, i, from the tunnel centerline. Moreover, the largest pullouts occur for restrained tees. Restraining the tee from pullout actually reduces the degrees of freedom available in the branch pipeline to accommodate lateral soil movement.
- Although DI pipelines have substantially higher capacity against leakage than CI pipelines at tees, some cases examined in this work show pullout on the order of 70 to 80% of push-on joint pullout capacity. Given the absence of pullout resistance in push-on joints, tees should always be checked as a potential risk with respect to tunneling induced ground deformation.

The observations and conclusions apply for CI and DI pipelines without significant corrosion and material defects. The effects of corrosion and defects are beyond the scope of this work, but should always be considered when evaluating pipeline performance in the field.

REFERENCES

ABAQUS 6.13. 2014. [Computer software]. Providence, RI, ABAQUS.

ASCE. 1984. *Guidelines for the seismic design of oil and gas pipeline systems*. Committee on Gas and Liquid Fuel Lifelines, American Society of Civil Engineers: Reston, VA.

ASTM. 2015. "Standard test methods for tension testing of metallic material." *E8/E8M-15a*, West Conshohocken, PA.

Attewell, P. B., Yeates, J., and Selby, A. R. 1986. *Soil movements induced by tunnelling and their effects on pipelines and structures*, Chapman & Hall, New York.

AWWA. 2009. "Ductile iron pipe, centrifugally cast, for water." *American Water Works Association Standard: ANSI/AWWA C151/A21.51-09*, Denver, CO.

Bouziou, D. 2015. *Earthquake-induced ground deformation effects on buried pipelines*. PhD Thesis. Cornel University, Ithaca, NY.

Cording, E. J. and Hansmire, W. H. 1975. "Displacements around soft ground tunnels." *General Report 5th Pan American Conference on Soil Mechanics and Foundation Engineering*, Buenos Aires, Session IV 571-632.

Cording, E. J. 1991. "Control of ground movements around tunnels in soil." *Proc. 9th Pan-American Conf. Soil Mech. Found. Engng, Valparaiso*, 2195–2244.

Davis, C. 2015. Resilience Manager, Los Angeles Department of Water and Power, personal communication.

Harris, C. W., and O'Rourke, T. D. 1983. "Response of jointed cast iron pipelines to parallel trench construction." *Geotechnical Engineering Rep. 83-5*, School of Civil and Environmental Engineering, Cornell Univ., Ithaca, NY.

Honegger, D. and Nyman, D. J. 2004. *Guidelines for the Seismic Design and Assessment of Natural Gas and Liquid Hydrocarbon Pipelines*. Pipeline Research Council International; Catalog No. L51927.

Hong, S. W. and Bae, G. J. 1995. "Ground movements associated with subway tunnelling in Korea." *Proc. Underground Construction in Soft Ground*. Rotterdam: AA Balkema, 229-232.

Johnson, J. B. 1890. "Cast-iron-strength, resilience, tests and specifications." *Trans. Am. Soc. Civil Eng.*, XXII(1), 91–120.

Jung, J.K., O'Rourke, T.D., and Argyrou, C. 2016. "Multi-directional force-displacement response of underground pipe in sand", *Can. Geotech. J. Special Issue on Pipeline Geotechnics.*

Jung, J. K., O'Rourke, T. D., and Olson, N. A. 2013a. "Uplift soil–pipe interaction in granular soil." *Can. Geotech. J.* **50**(7), 744-753.

Jung, J. K., O'Rourke, T. D., and Olson, N. A. 2013b. "Lateral soil-pipe interaction in dry and partially saturated sand." *J. of Geotech. Geoenviron. Engng ASCE.* **139**(12), 2028-2036.

Klar, A. and Marshall, A. M. 2015. "Linear elastic tunnel pipeline interaction: the existence and consequence of volume loss equality." *Géotechnique.* **65**(9), 788-792.

Klar, A., Vorster, T. E. B., Soga, K. and Mair, R. J. 2005. "Soil–pipe interaction due to tunnelling: comparison between Winkler and elastic continuum solutions." *Géotechnique.* **55**(6), 461–466.

Klar. A., Vorster, T.E.B., Soga, K., and Mair, R.J. 2007 "Elastoplastic solution for soil-pipe-tunnel interaction", *J. Geotech. Geoenviron. Engng* **133(**7), 782–792.

Klar, A., Marshall, A. M., Soga, K. and Mair, R. J. 2008. "Tunneling effects on jointed pipelines." *Can. Geotech. J.*, **45**(1), 131–139.

Lake, L. M., Rankin, W. J., and Hawley, J. 1996. *Prediction and effects of ground movements caused by tunnelling in soft ground beneath urban areas*. CIRIA.

Lilliefors, H. W. 1967. "On the Kolmogorov-Smirnov test for normality with mean and variance unknown." *Journal of the American Statistical Association*, **62(**318), 399-402.

Mair, R. J., Taylor, R. N. and Bracegirdle, A. 1993. Subsurface settlement profiles above tunnels in clays." *Géotechnique.* **43**(2), 315-320.

Mair, R. J. and Taylor, R. N. 1997. Bored tunnelling in the urban environment. *Proc. 14th Int. Conf. Soil Mech. Found. Engng, Hamburg,* **4**, 2353–2385.

Marshall, A. 2009. *Tunnelling in sand and its effect on pipelines and piles.* PhD Thesis, Engineering Department, University of Cambridge, UK.

Marshall, A., Klar, A., and Mair, R. 2010. "Tunneling beneath buried pipes: view of soil strain and its effects on pipeline behavior." *J. Geotech. Geoenviron. Engng* **136(**12), 1664-1672.

Marshall, A., Farrell, R., Klar, A., and Mair, R. 2012. "Tunnels in sands: the effect of size, depth and volume loss on Greenfield displacements." *Géotechnique*. **62**(5), 385–399.

Massachusetts Administrative Code, Public Utilities. 2006. Title 220, Section 113.

New York Administrative Code, Public Services. 2006. Title 16, Section 255.757.

O'Reilly, M. P. and New, B. M. 1982. "Settlements above tunnels in the United Kingdom: their magnitude and prediction*." Proc. Tunnelling '82, Brighton*, 173–181.

O'Rourke, T. D. 2010. "Geohazards and large geographically distributed systems." 2009 Rankine Lecture. *Géotechnique.* **60**(7), 503-543.

O'Rourke, T. D., Jezerski, J. M., Olson, N. A., Bonneau, A. L., Palmer, M. C., Stewart, H. E., O'Rourke, M. J., and Abdoun T. 2008. "Geotechnics of pipeline system response to

earthquakes." *Geotech. Earthquake Engng. and Soil Dynamics IV (GEESD)*, Sacramento, CA.

O'Rourke, T. D., Jung, J. K. and Argyrou, C. 2015. "Underground infrastructure response to earthquake-induced ground deformation." *Proc. 6th Int. Conf. on Earthquake Geotech. Eng.* Christchurch.

O'Rourke, T. D. and Kumbhojkar, A. S. 1984. *Field Testing of Cast Iron Pipeline Response to Shallow Trench Construction*. Cornell University.

O'Rourke, T. D., Netravali, A. N., Pendharkar, S. M., Toprak, S., Tonkinson, A., and Chaudhuri, D. 1996. "Evaluating service life of anaerobic joint sealing products and techniques." *Final Rep. 96/0318*, Gas Research Institute, Chicago.

O'Rourke, T. D., and Trautmann, C. H. 1980. "Analytical modeling of buried pipeline response to permanent earthquake displacements." *Rep. 80-4, School of Civil and Environmental Engineering*, Cornell Univ., Ithaca, NY.

Osman, A. S., Mair, R. J., and Bolton, M. D. 2006. "On the kinematics of 2D tunnel collapse in undrained clay." *Géotechnique.* **56**(9), 585-595.

Peck, R. B. 1969. "Deep excavations and tunnelling in soft ground." *Proc. 7th Int. Conf. Soil Mech. Found. Engng., Mexico City*, 225–290.

Pipeline Safety and Hazardous Materials Administration [PHMSA]. 2015. Data and Statistics http://www.phmsa.dot.gov/pipeline/library/data-stats (accessed 30 Nov. 2015).

Prior, J. C. 1935. *Investigation of bell and spigot joints in cast-iron water pipes. Part I-Pullout strength. Part II-Bell strength. Part III-Harness strength*, College of Engineering, Ohio State Univ., Columbus, OI.

Rajani, B. and Abdel-Akher, A. 2013. "Performance of cast-iron-pipe bell-spigot joints subjected to overburden pressure and ground movement." *J. Pipeline Syst. Eng. Pract. ASCE* **4**(2), 98-114.

Schlick, W. J. and Moore, B. A. 1936. "Strength and elastic properties of cast iron in tension, compression, flexure, and combined tension and flexure," *Bulletin 127*, Iowa Engineering Experiment Station, Ames, IA.

Stewart, H. E., O'Rourke, B. J., O'Rourke, T. D., and New, B. M. 1989. "Evaluation of cast iron pipeline response at excavation crossings." *Geotechnical Engineering Rep. 89-1*, School of Civil and Environmental Engineering, Cornell Univ., Ithaca, NY.

Taki, H., and O'Rourke, T. D. 1984. "Factors affecting the performance of cast iron pipe." *Geotechnical Engineering Rep. 84-1*, School of Civil and Environmental Engineering, Cornell Univ., Ithaca, NY.

Vorster, T. E. B., Klar, A., Soga, K. and Mair, R. J. 2005. "Estimating the effects of tunneling on existing pipelines." *J. Geotech. Geoenviron. Engng* **131(**11), 1399–1410.

Wang, Y., Shi, J., and Ng, C. W. W. 2011. "Numerical modeling of tunneling effect on buried pipelines." *Can. Geotech. J.*, **48**(7), 1125-1137.

Wham, B. P. 2016. *Jointed pipeline response to large ground movements.* PhD Thesis. School of Civil and Environmental Engineering, Cornell University, Ithaca, NY.

Wham, B. P. and O'Rourke, T. D. 2015. "Jointed pipeline response to large ground deformation." *J. Pipeline Syst. Eng. Pract.,* 04015009.

Zhou, B. 2014. *Tunelling-induced ground displacements in sand*. PhD Thesis, Department of Engineering, University of Nottingham, Nottingham, UK.

LIST OF FIGURES

FIGURES

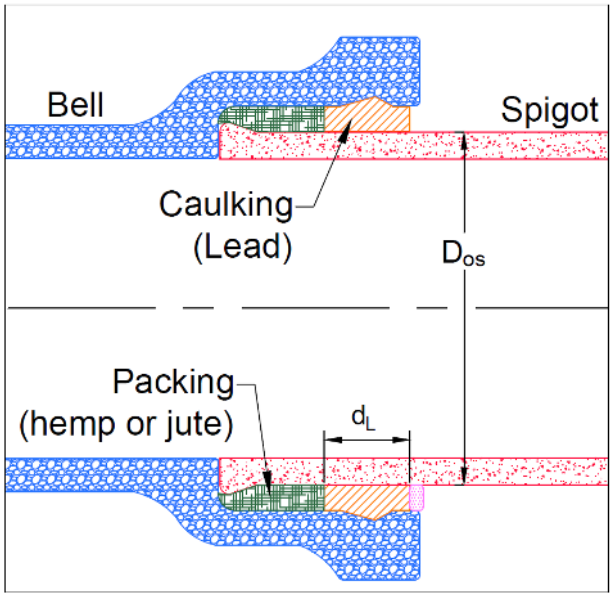

Figure 1. Cross-section of a typical CI joint

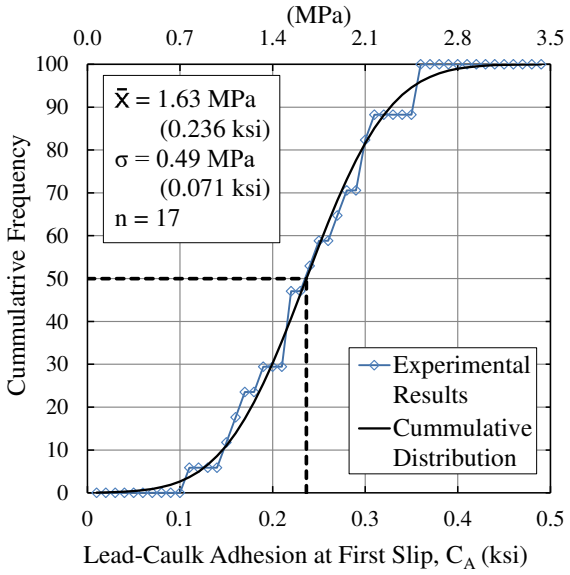

Figure 2. Cumulative frequency plot of CI-lead adhesion at first leakage in CI joints

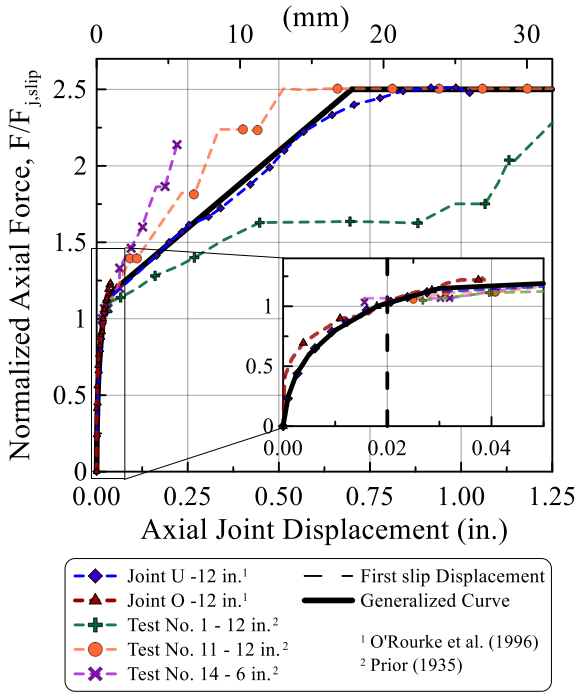

Figure 3. Normalized joint pullout force vs. axial displacement for lead-caulked CI joints

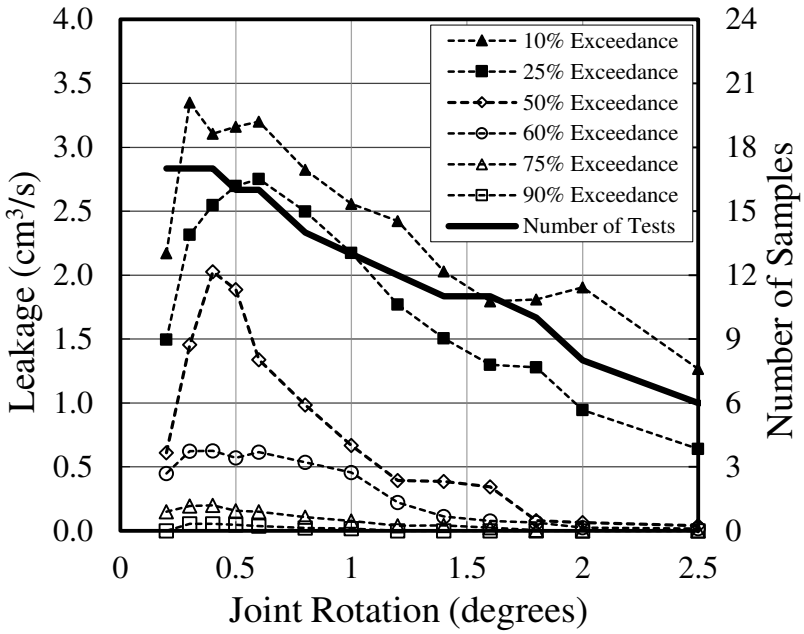

Figure 4. Sample size and leakage rate exceedance levels for 100, 150, and 200-mm (4, 6, and 8-in.) diameter CI joint specimens (adapted from Harris and O'Rourke 1983)

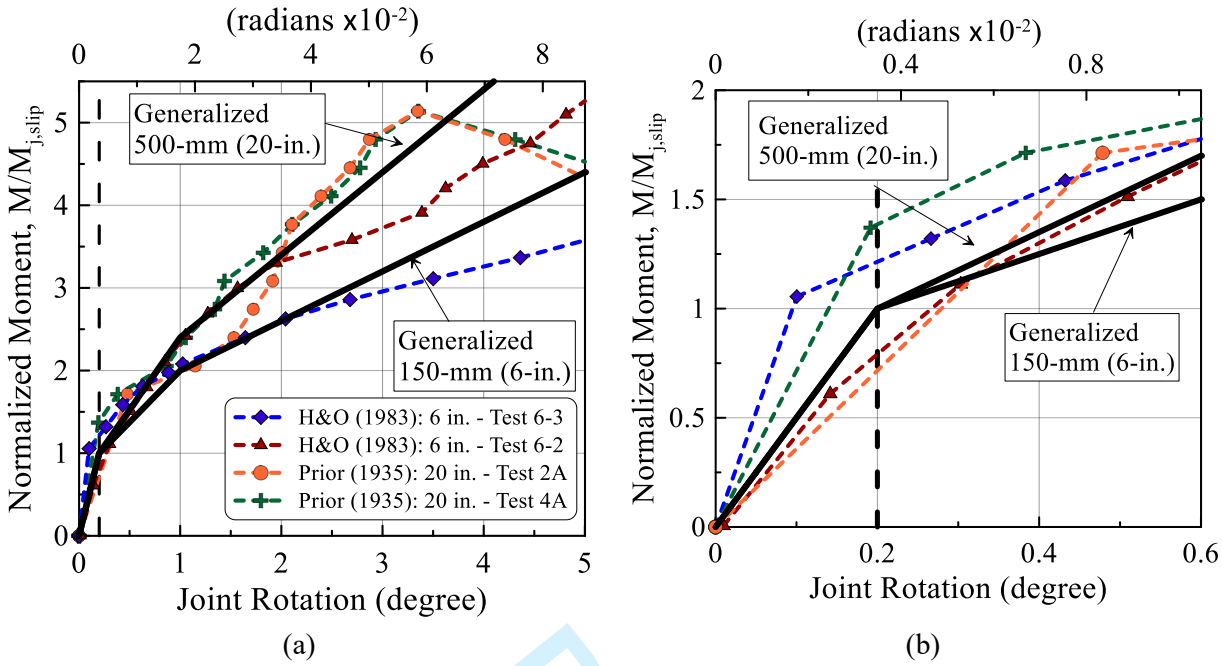

Figure 5. (a) Normalized moment-rotation relationships for 150 and 500-mm (6 and 20-in.) diameter CI joints and (b) expanded view of rotation at first slip

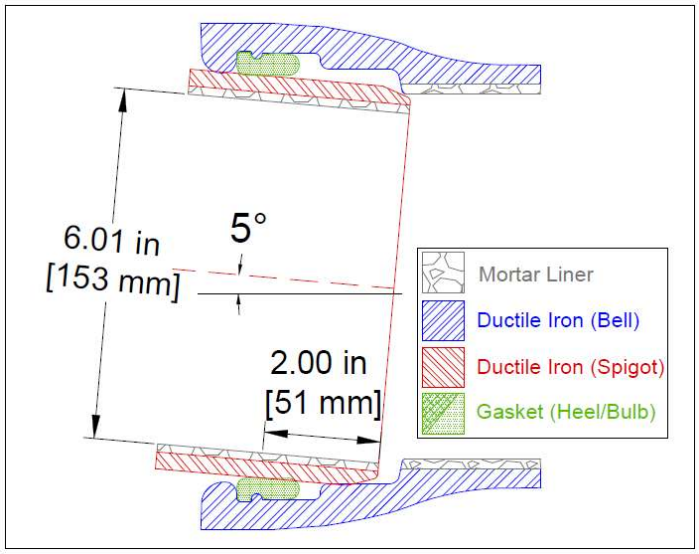

Figure 6. Typical 150-mm (6-in.) DI Joint cross-section with 5° rotation

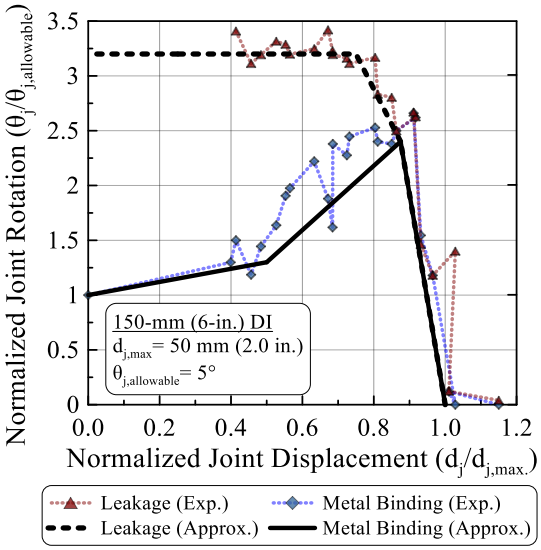

Figure 7. Pressure boundary for leakage of 150-mm (6-in.) diameter DI joint as a function of normalized joint rotation and axial displacement (adapted from Wham and O'Rourke 2015)

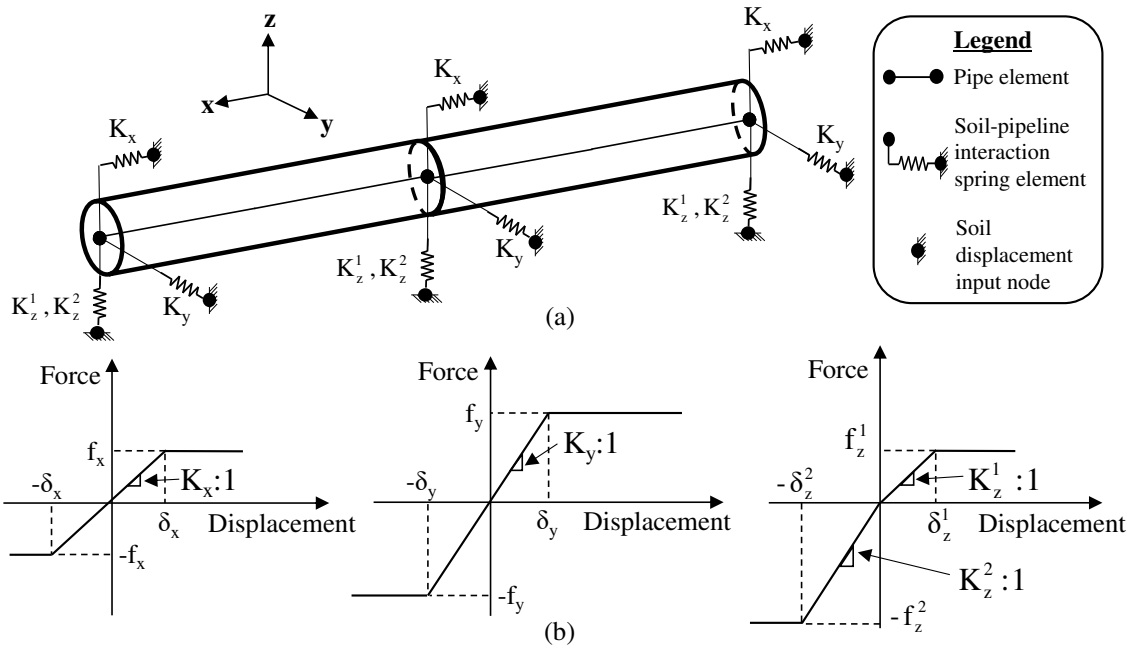

Figure 8. (a) Schematic of FE model and (b) bilinear force vs. displacement relationships at pipe-soil interface based on the elasto-plastic models recommended by ASCE (1984) and Honegger and Nyman (2004) [after Bouziou 2015]

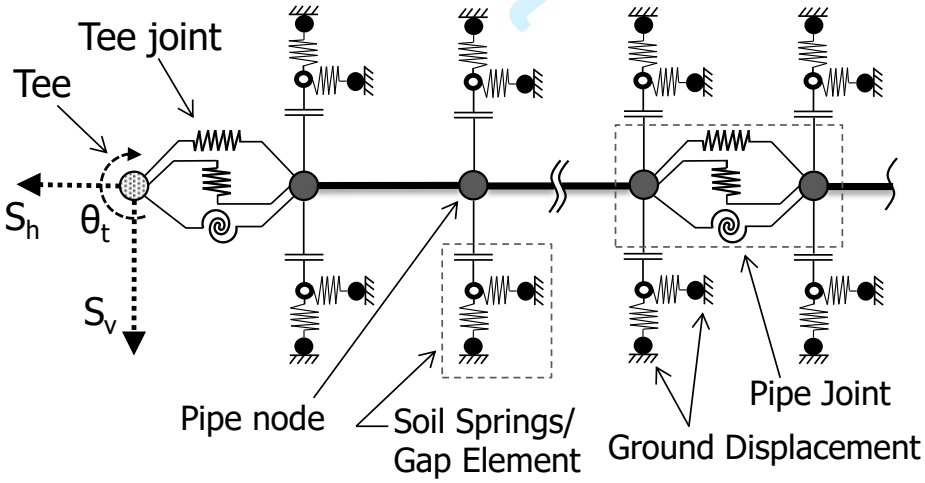

Figure 9. Schematic of enhanced 2D FE model including tee joint

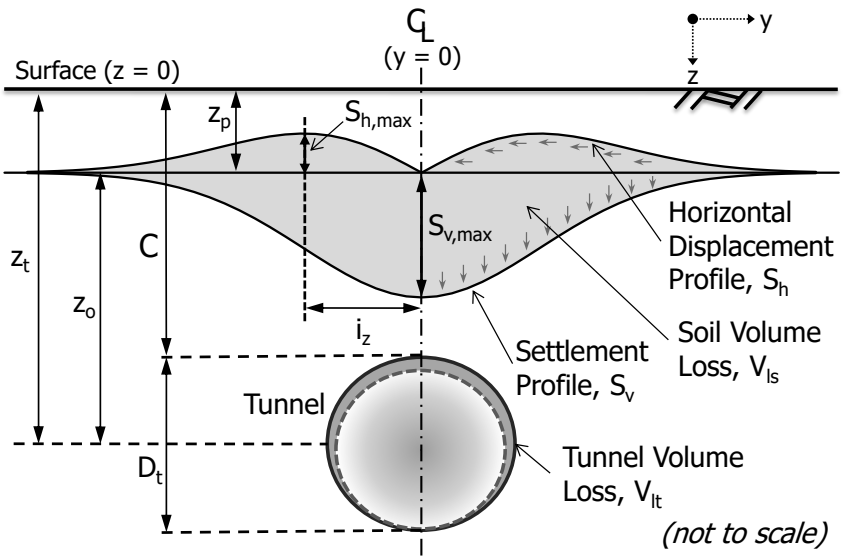

Figure 10. Transverse view of tunnel with settlement and horizontal movement distributions at depth of pipeline

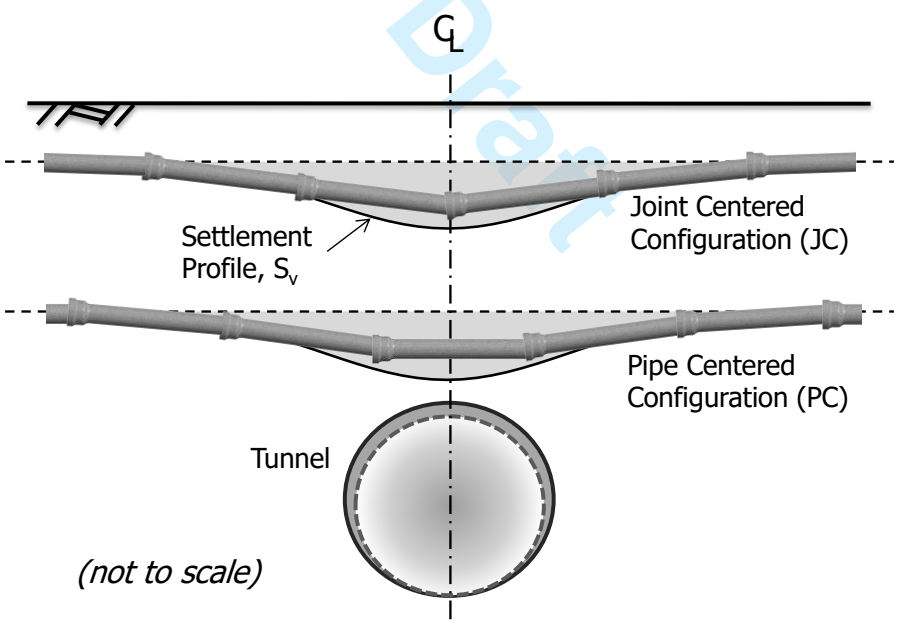

Figure 11. Illustration of joint centered and pipe centered pipeline configurations

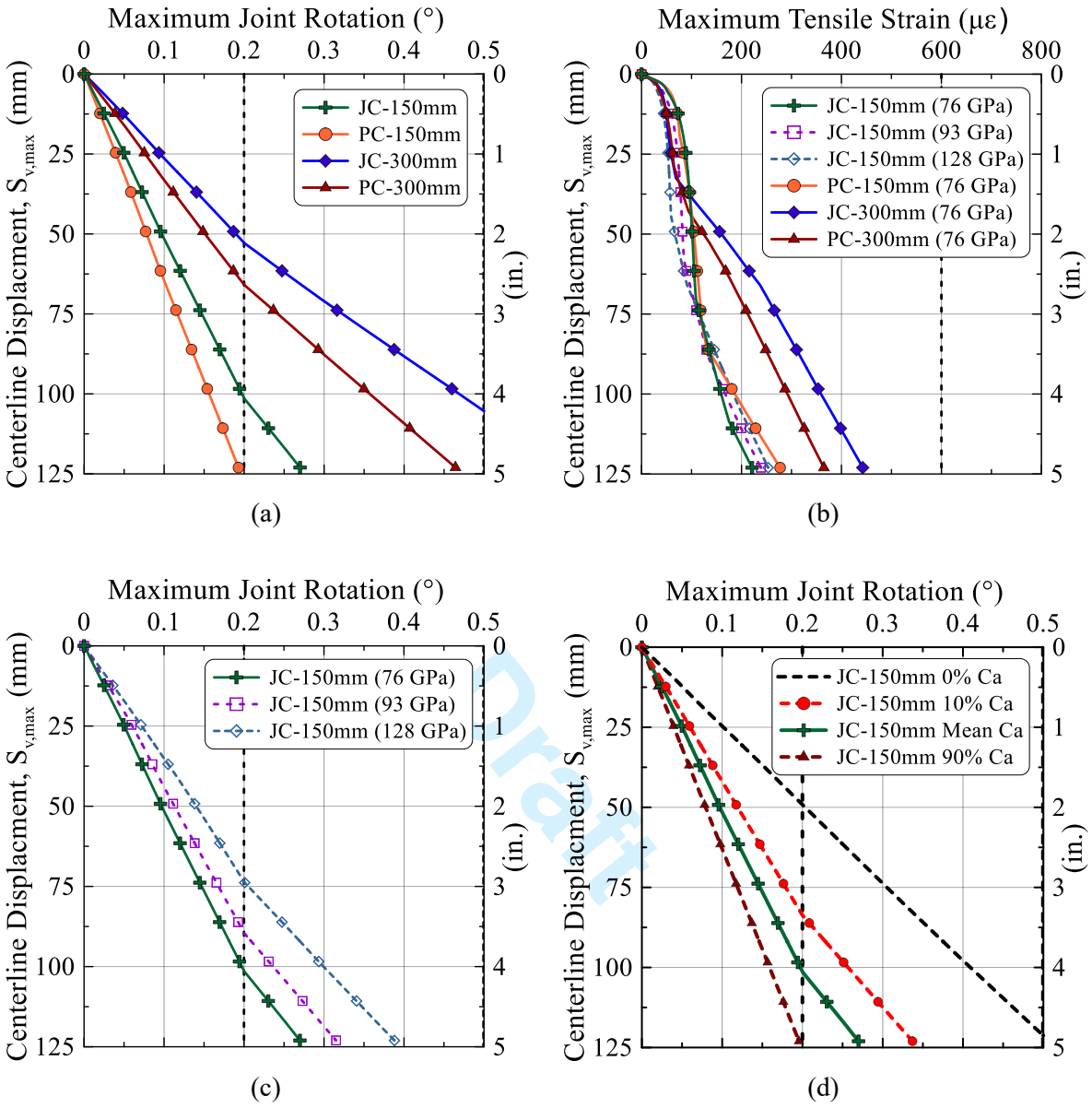

Figure 12. Continuous jointed CI pipeline results for clay settlement profile: (a) maximum joint rotation, (b) maximum tensile strain, (c) 150-mm (6-in.) joint rotation with varying CI modulus, and (d) maximum joint rotation for JC 150-mm (6-in.) with varying CI-lead adhesion, C_A

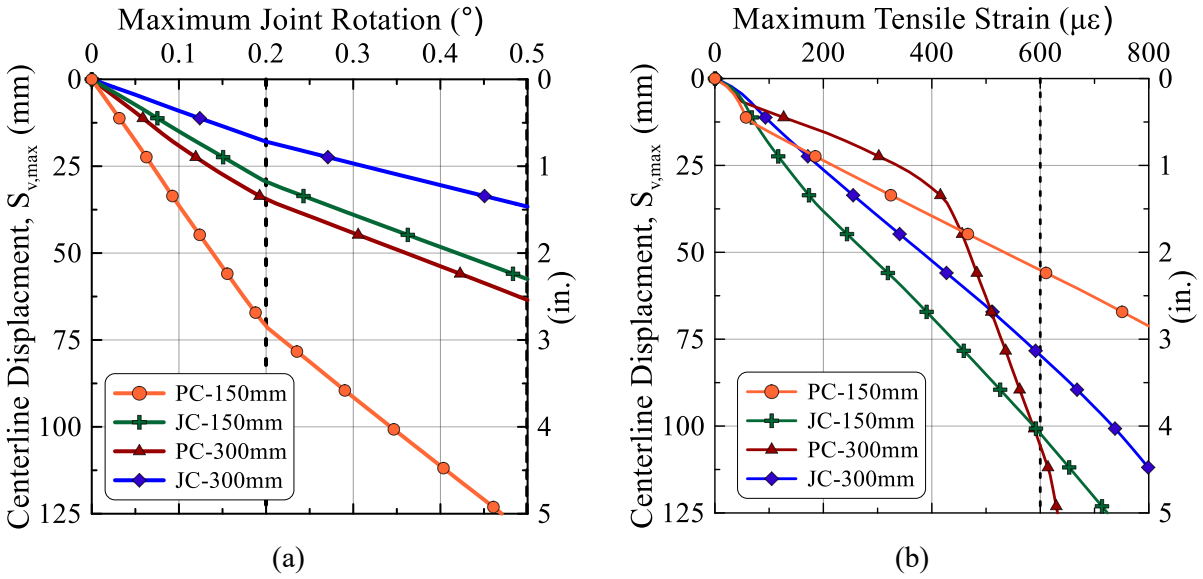

Figure 13. Maximum (a) joint rotation and (b) tensile strain along continuous jointed CI pipeline for joint centered and pipe centered configurations in sand settlement profile

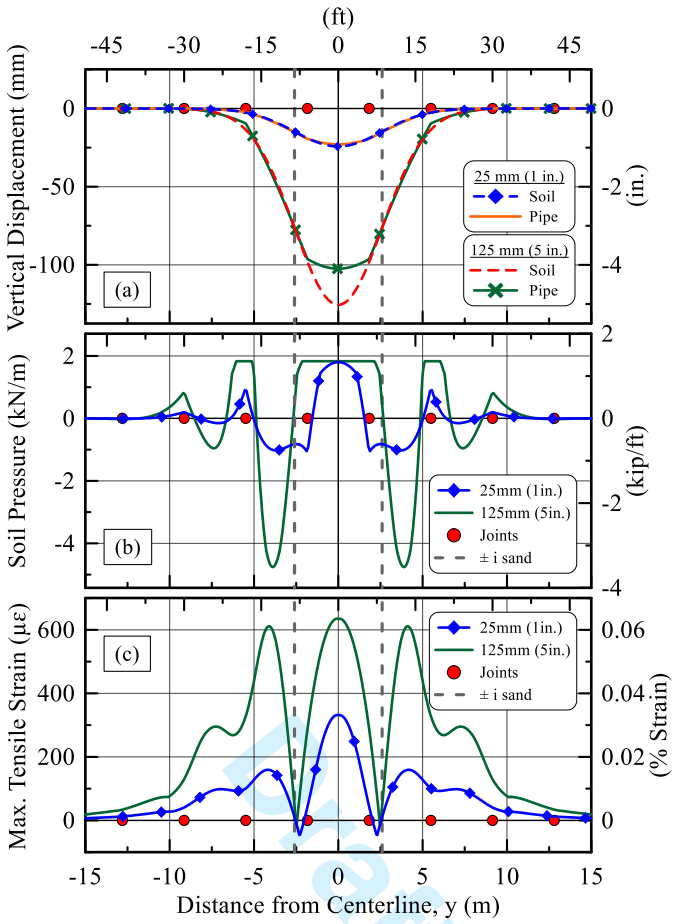

Figure 14. Continuous jointed 300 mm CI pipe (a) vertical displacement, (b) soil pressure, and (c) maximum tensile strain vs. distance from tunnel centerline at vertical displacements of 25 and 125 mm (1 and 5 in.) in sand

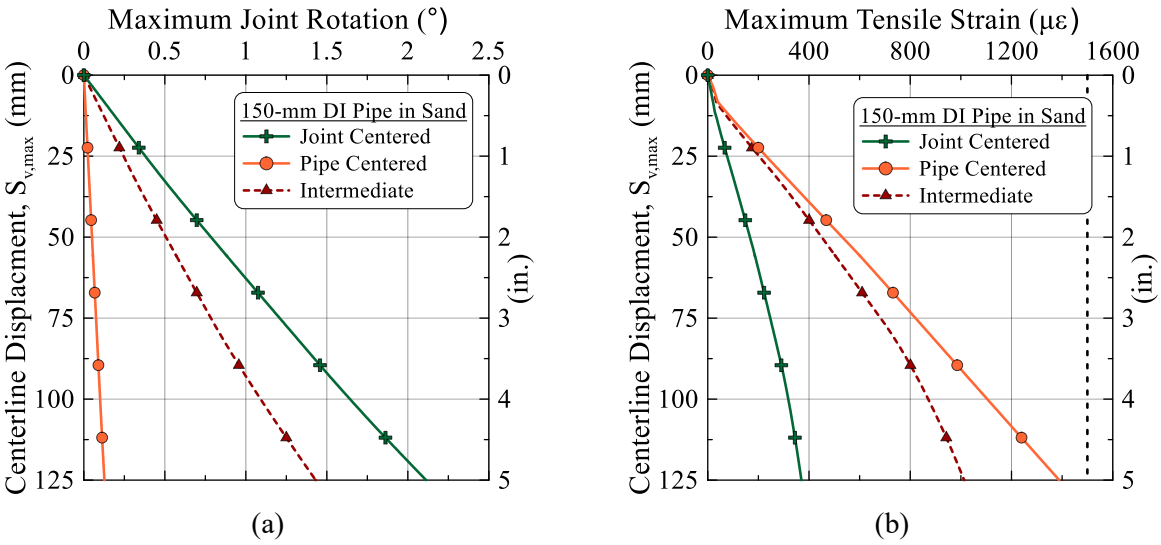

Figure 15. Maximum (a) joint rotation and (b) tensile strain results of 150-mm (6-in.) continuous DI pipe for joint and pipe centered configurations in sand profile

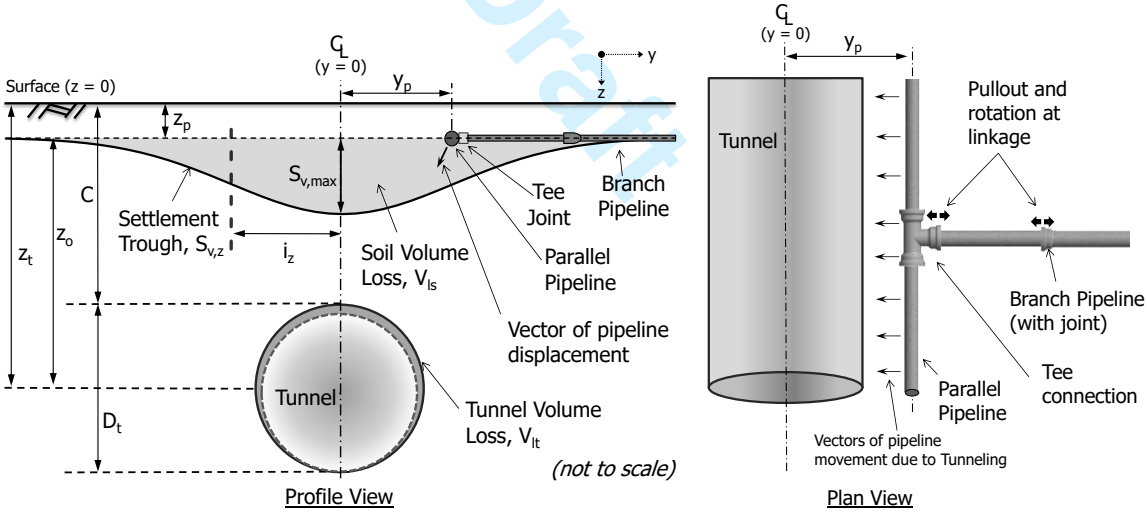

Figure 16. Illustration of tunnel cross-section, settlement trough and parallel pipeline with tee connection

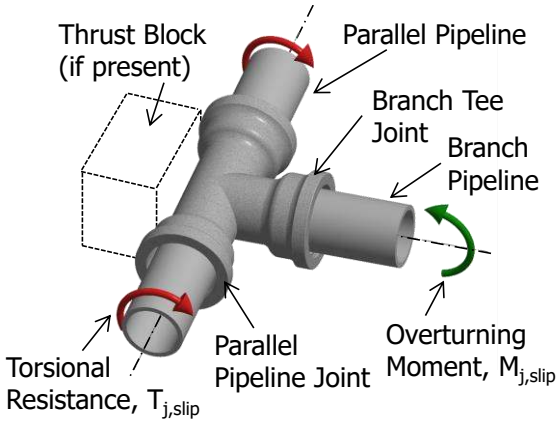

Figure 17. 3D illustration of typical CI tee joint

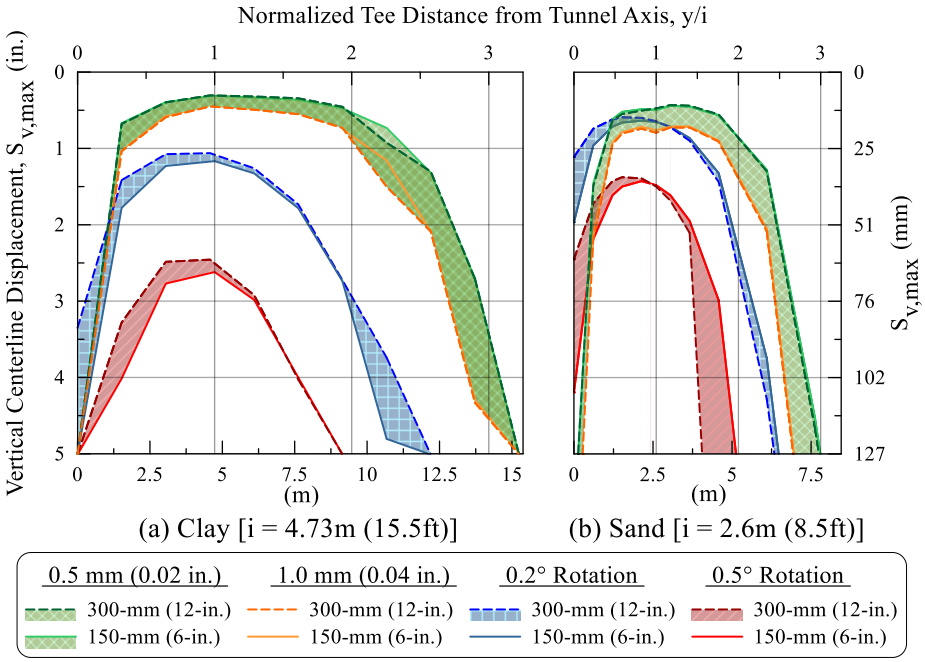

Figure 18. Centerline settlement in clay and sand associated with exceeding CI tee pullout and rotational limits as a function of tee location from the tunnel centerline

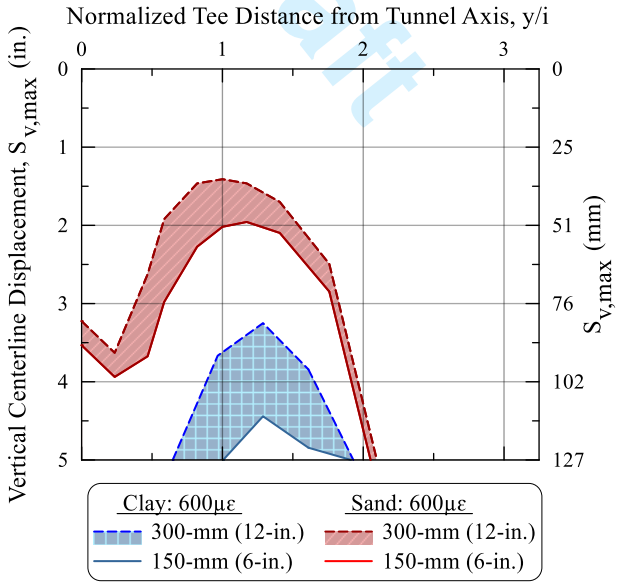

Figure 19. Centerline settlement in clay and sand associated with exceeding the allowable CI tensile strain as a function of tee location from the tunnel centerline

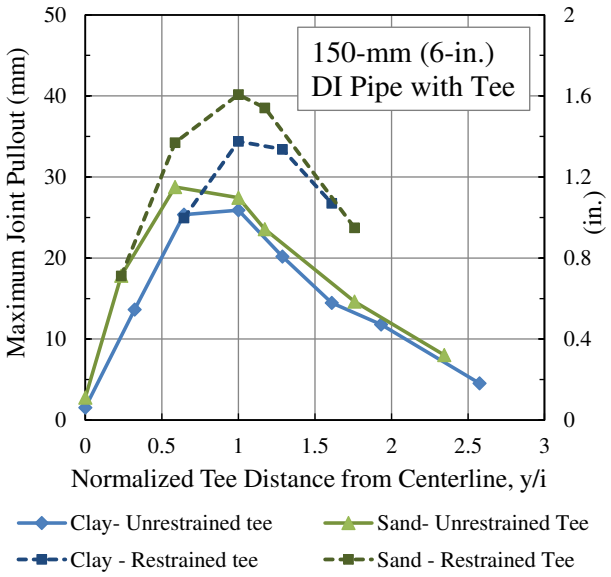

Figure 20. Maximum DI joint pullout in clay and sand as a function of normalized tee location